Thermal fatigue behaviour of WC-20Co and WC-30(CoNiCrFe) cemented carbide

L. Emanuelli[a], M. Pellizzari[a], A. Molinari[a], F. Castellani[b], E. Zinutti[b]

[a] Dpt. Industrial Engineering, University of Trento, Via Sommarive 9, 38123 Trento, Italy

[b] SMS Meer S.p.A, Via Udine 103, 33017 Tarcento (UD), Italy

Abstract

Cemented carbides are used in many applications, such as drawing dies, cutting tools and hot rolls. In applications where cyclic temperature variations are present, an important factor that must be taken into account is thermal fatigue (TF). In this study, TF behaviour of two commercial cemented carbides was evaluated by means of a custom test configuration inducing a biaxial state of stress. At an early stage of the damage process, crack density is higher in WC-30(CoNiCrFe), whilst crack length is lower than WC-20Co. At a later stage cracking proceeds by propagation of existing cracks, partly reducing the difference between the two grades. The prevailing fracture modes are different in the two materials. In WC-20Co the main fractures occur at the WC/WC grain boundary and at WC/Co interface. In WC-30(CoNiCrFe) cracking proceeds by fracture of carbide particles and shear fracture of binder phase. A possible influence of oxidation on the TF crack propagation has been evidenced.

Keywords

Cemented carbide; thermal fatigue; crack propagation; oxidation

1 Introduction

Cemented carbide is a composite material formed by high fraction of hard WC particles bonded by a soft and ductile Co binder. This material has outstanding properties of high hardness and wear resistance. Mechanical properties are strongly related to microstructure, namely to the binder content

and carbide grain size. An increase in binder content and WC grain size leads to a decrease of hardness, and to an increase in the fracture toughness [1][2], while transversal rupture strength rises up to a maximum and then diminishes [3]. For this reason it is possible to tailor the properties in relation to specific applications by changing the microstructural parameters.

Cemented carbide components undergo TF damage in several applications involving rapid temperature variations leading to strong thermal gradients. TF is a typical oligo-cyclic fatigue phenomenon [4], which promotes the surface initiation of a fine crack network generally showing a small penetration depth (tenth of mm). In most cases, this damage (*heat checking* is the name used to identify the crack network) leads to the deterioration of tool surface finishing, which is generally followed by that of the worked material. Only rarely TF alone may cause catastrophic failure, but the presence of a secondary damage phenomenon (e.g. wear, contact fatigue...) enhance crack propagation promoting a premature loss of structural integrity. From an industrial point of view, the selection of a most appropriate material or/and the development of best operational practices are necessary in order to avoid or delay the effective damage.

In an empirical way, by means of the theory of thermo-elasticity and fracture mechanics, it is possible to correlate the thermal shock (TS) resistance of cemented carbide to the parameter $kTRS/E\alpha$, where TRS is the transverse rupture strength, k is the thermal conductivity, E is Young's modulus, and α is the coefficient of thermal expansion [1][5]. This parameter is often used preliminarily to predict the TF resistance as well. It is clear that the influence of microstructural parameters on the TS resistance, and even more on the TF resistance, is very complex. In spite of this, a few authors have studied the TF resistance of cemented carbides. Tumanov et al. [6] found that, when the cemented carbide is subjected to repeated TS, micro-stresses are formed in the material because of a difference in thermal expansion coefficients of the WC and Co phases. A reduction in the Co content leads to a reduction in the TS resistance because of an increase in tensile stresses in the metal matrix. In the case of TF behaviour of a cemented carbide hot roll, Lagerquist [7] reached the following conclusions: an increase in the cobalt content and in the WC grain size leads to an increased number of cracks but to

a decreased propagation rate. However the influence of grain size becomes fundamental only in case of low amount of cobalt. The common fracture modes that can occur in the cemented carbides are cleavage of WC particles, fracture at the WC/WC grain boundary and at the WC/Co interface and shear fracture of binder phase. The ratio of transgranular/intergranular fracture of WC increases with a rise of the WC grain size [3]. Cracks nucleate at the surface and their propagation occurs preferentially at the WC/WC grain boundary and the WC/Co interface due to higher propagation rate. Ning et.al. stated that thermal cracking proceeds by nucleation, growth and aggregation of microvoids at the interface between WC and the Co matrix [8]. The overall damage was found to be proportional to the maximum temperature during cycling and a higher cooling rate favoured more pronounced cracking. Ishihara confirmed a similar mechanism for 72WC-8TiC-8TaC-2NbC-10Co and stated that cracks mostly propagate inside the metal binder or at the interface with the WC phase, following a zigzag path [9].

Another important parameter, which must be considered in applications with rapid temperature variations, is the oxidation resistance. Most of the data regarding oxidation resistance of WC-Co alloys are related to a temperature range between 500-1000°C in different atmospheres (air, Ar/O_2 mixture or O_2) [10][11][12][13][14][15]. In all cases, WO_3, $CoWO_4$ and Co oxides were formed during the oxidation. An increase in the binder content leads to an improved oxidation behaviour because of a higher amount of $CoWO_4$ that is denser and more protective than the WO_3. After L.Chen et al. [16] the oxidation of Co occurs before that of WC, which is contrary to the thermodynamic calculations. This is justified taking into account differences in oxidation kinetics of WC and Co. Voitovich et al. [14] also studied the effect of partial and complete substitution of Co by Ni. In the temperature range between 500 and 800°C the oxidation of Co is higher than that of Ni. Ni is not suitable to moderate the rate of oxygen interaction with WC and leads to a reduction of the oxidation resistance since WO_3 becomes the main oxidation product. Aristizabal et al. [17][18][19] confirm the increase of the oxidation resistance increasing the binder content and the decrease of the passivation

effect by increasing Ni/Co ratio. Nevertheless, the negative effect due to the introduction of Ni is negligible in case of 15 wt.% binder and becomes important in case of 25 wt.% binder.

Few data are available in literature on the TF resistance of cemented carbides that contain a high Co content. The aim of the present study was to evaluate the TF resistance of two commercial cemented carbides by means of a custom test configuration inducing a biaxial state of stress in a harsh oxidizing environment.

2 Materials and methods

Two different commercial cemented carbide grades containing 20wt.%Co (WC-20Co) and 19wt.%Co-9.5wt.%Ni-1wt.%Cr-0.5wt.%Fe (WC-30CoNiCrFe) were selected for present investigation. A complete microstructural characterization was carried out after proper metallographic preparation. Murakami's reagent (100 ml distilled water, 5-10g KOH or NaOH, 5-10g $K_3[Fe(CN)_6]$) [20], was used for selective etching of WC particles. Composition of the two materials was investigated by EDAX analysis. Mean grain size (D_{WC}), contiguity (C) and mean binder free path (λ) were determined by using SEM micrographs at 3000X of magnification. Contiguity measures the carbide contacts and the mean binder free path is the average thickness of cobalt between the WC particles. These parameters are defined by equations (1), (2) and (3) [21][22].

$$D_{WC} = \sum_{i}^{n} l_i^4 / \sum_{i}^{n} l_i^3 \qquad (1)$$

$$C = 2 \times (N_L)_{WC\text{-}WC} / (2 \times (N_L)_{WC\text{-}WC} + (N_L)_{WC\text{-}Co}) \qquad (2)$$

$$\lambda = 2 \times f_{V\_Co} / (N_L)_{WC\text{-}Co} \qquad (3)$$

where

l_i: measured intercept length;

$f_{V_{Co}}$: Co volumetric fraction;

n: numbers of WC grains intercepted;

L: length of the test line;

N_L: number of WC-WC grain boundaries or WC-Co interfaces intercepted per unit length.

The method used to measure these microstructural parameters is the “Linear intercept method”.

At least 200 grains were considered each image, as well as at least 20 grains were crossed by the test line, as recommended by the method to get a statistically significant result. C and λ were measured for each test line and, finally, mean C and mean λ with the respective standard deviation were calculated.

TF tests were carried out using the experimental configuration shown in details in Figure 1 [23]. A disc specimen (40 mm external diameter, 20 mm width) continuously rotating at 4rpm was induction heated up to 600°C and subsequently cooled down to 80°C by a water jet (18°C, 2 l/min). The maximum temperature of 600°C at the exit of the inductor, monitored by an infrared pyrometer, was chosen referring to the typical temperature reached in many commercial applications involving rapid temperature variations. This also holds for carbide tools coming in contact with materials hot worked at temperature much higher than 600°C, but for a very short time, so that thermal equilibrium conditions cannot be established. Furthermore, according to literature, 600°C is the maximum operating temperature of cemented carbides, in view of the significant mechanical strength and hardness reductions observed above this temperature [24]. Heating was limited to a portion of the outermost surface, individuated by an angle of 105° and 10mm width, so to induce thermal gradients in both, tangential and axial direction. The resulting biaxial state of stress allowed the formation of a crack network, similar to that observed in many components undergoing TF during service. TF cracks on the WC-30(CoNiCrFe) surface started to be visible at 1300 cycles, with a 200X SEM magnification. For this reason, 3 tests were carried out up to 3000 cycles, with interruptions after

1300 and 2000 cycles to monitor the damage evolution. Thermal cracking was evaluated by means of quantitative analysis on more than 10 scanning electron microscopy images of the surface.

An automated image-processing route was set up using a Leica Qwin software in order to measure the total crack length and the number of the cracks for each SEM micrograph. The mean surface crack length (total surface crack length divided by the number of cracks) and the crack density (number of cracks divided by the reference area) are the average values of three different tests. The damage mechanisms and the oxidation phenomena were further investigated analysing a cross sectional view of the sample by SEM, to investigate the in-depth propagation of cracks. In order to preserve the surface region and the oxide scales from damage during EDM cutting and metallographic preparation, samples were preliminarily nickel-plated. Oxidation kinetic was evaluated by means of thermogravimetric analysis. The two carbides were oxidized isothermally in an air flux at 500 and 600°C for 2h. 600°C is the maximum TF test temperature while 500°C was chosen in order to evaluate the oxidation evolution in case of a lower kinetic. HV10 hardness tests were carried out, according to UNI EN ISO 6507, in order to analyse any possible thermal softening effect during TF test. Provided that the induction heated is about 2mm in depth the hardness profiles was obtained using 3 indentations for each distance.

3 **Results and discussion**

3.1 Microstructural analysis

Figure 2 shows the microstructure of the two materials. The different size of WC particles and binder content are evident. The microstructural parameters D_{wc}, mean C and mean with standard deviations are reported in Table 1.

Materials	D_{WC} (μm)	C (-)	λ (μm)
WC-20Co	2.65	0.53 ± 0.10	1.41 ± 0.19
WC-30(CoNiCrFe)	4.71	0.43 ± 0.11	3.54 ± 0.41

Table 1: microstructural parameters of WC-20Co and WC-30(CoNiCrFe)

Increasing the binder content, the mean binder free path increases and contiguity decreases, since the carbide spatial coincidence decreases. Moreover, the WC-30(CoNiCrFe) shows a higher grain size.

3.2 *TF damage*

Figure 3 shows the surface of the disks after 1300, 2000 and 3000 TF cycles.

TF damage leads to nucleation and propagation of new cracks. After a certain number of cycles, an increase in the crack density and in the mean crack length brings about the formation of a mesh. Comparing the two commercial materials, it is possible to highlight different damage behaviour. WC-30(CoNiCrFe) is characterized by high nucleation rate that brings about the formation of many small cracks that are slightly branched. Only at 3000 cycles, the formation of a mesh occurs due to an increased crack density and a reduced propagation rate. Differently, WC-20Co presents a high propagation rate to the detriment of a low nucleation rate. A reduced number of long branched cracks is formed on the WC-20Co after 1300 cycles. Increasing the cycles number, the crack density does not change while mean crack length and ramification increase. Already after 2000 cycles, cracks start to interconnect from each other and, at 3000 cycles, form a mesh. The high propagation rate in case of WC-20Co leads to a great crack extension on the surface and in the depth. The following analyses give confirmation of these different damage behaviours.

Figure 4a and 4b show the variation of mean crack length and of the crack density with the number of cycles for the two materials, respectively.

The mean crack length increases with of the number of cycles, but the increase until 2000 cycles is higher in the case of WC-20Co. After 2000 cycles, WC-20Co shows a plateau and differently, in the

case of WC-30(CoNiCrFe), the mean crack length increases quickly. At 3000 cycles the two materials present similar values. After an initial transient period, the crack density in WC-20Co reaches a steady value, whilst, in WC-30(CoNiCrFe), it increases up to a maximum value and than decreases. These different behaviours are justified taking into account that an increase in the binder content leads to an increase in toughness, which results in a lower propagation rate. This condition promotes the possible nucleation of new cracks, since shorter cracks preserve the local constraint inducing higher thermomechanical stresses [8]. In other words, the propagation of long thermal cracks allows the free deformation in their neighbourhood and avoids the nucleation of new cracks as confirmed by the inverse correlation between mean crack length and crack density (Figure 4c). This behaviour can be explained by the influence of microstructure on the crack density and the mean crack length. A decrease of the contiguity and an increase of the mean binder free path lead to reduced crack length and to increased crack density (Table 1). Figure 5a and 5b show the cross section of the two specimens after 3000 cycles, to highlight the cracks propagating in depth and the crack width.

WC-20Co is characterized mainly by straight sharp cracks whilst the WC-30(CoNiCrFe) exhibits more tortuous crack paths, synonymous of a slower propagation. This is clearly confirmed by the higher penetration depth and crack width measured in WC-20Co than in WC-30(CoNiCrFe) (Table 2). This evidence practically extends the result found for the surface crack propagation also to the in depth propagation. I.e. higher penetration depth means low value of crack density because of a reduction of the local constraint.

Materials	depth (μm)	width (μm)
WC-20Co	142 ± 25	22 ± 12
WC-30(CoNiCrFe)	70 ± 14	16 ± 5

Table 2: the penetration depth and the width of the cracks after 3000 cycles for WC-20Co and WC-30(CoNiCrFe) cemented carbides

In presence of a lower amount of binder, cracks propagate approximately parallel to the temperature gradient, i.e. perpendicular to the external surface. Differently, deviations and branching of cracks occur in presence of an increasing binder amount [7]. In this case, the slower propagation may also induce a stronger interaction with oxidizing phenomena, as evidenced in the next paragraph.

Figure 5c highlights that fractures at the WC/WC grain boundary and at WC/Co interface are the main mechanisms in WC-20Co. On the other hand, the cleavage fracture of WC particles and shear fracture of binder phase are the prevailing propagation mechanisms in WC-30(CoNiCrFe), as shown in Figure 5d. This different behaviour is justified taking into account that the ratio of transgranular/intergranular fracture of WC increases with a rise of the WC grain size [3]. Differently, increasing the binder content, cracks are more often forced to propagate in the binder phase because of a reduction of the contiguity and a higher mean binder free path [7]. In view of this evidences, the correlation highlighted in Figure 4c is now more directly associated to the different microstructures of the two materials. The hardness values at the surface and at the core of the two materials are the same (Table 3), highlighting that there is no softening effect due to the high temperature reached. This means that the TF damage is not correlated with a decrease of mechanical properties due to high temperature.

WC-20Co		WC-30(CoNiCrFe)	
distance (mm)	hardness (HV10)	distance (mm)	hardness (HV10)
1.32	844 ± 12	0.92	713 ± 8
2.69	845 ± 6	1.82	693 ± 7
4.05	836 ± 5	3.23	704 ± 7
5.88	829 ± 15	4.51	704 ± 13
7.61	840 ± 13	5.78	703 ± 6
9.29	835 ± 5	7.63	706 ± 8
10.94	837 ± 18	8.64	709 ± 10

Table 3: hardness profiles from the surface to the core for WC-20Co and WC-30(CoNiCrFe)

3.3 Oxidation behaviour

Thermogravimetric analysis at 500°C and 600°C for 2h were conduced in order to understand the possible effect of the oxidation on the TF damage.

Parabolic rate constant $mg^2/(cm^4min)$		
T(°C)	*WC-20Co*	*WC-30(CoNiCrFe)*
500	0,11E-03	0,15E-03
600	8,30E-03	2,44E-03

Table 4: Parabolic rate constant of WC-20Co and WC-30(CoNiCrFe) at 500°C and 600°C

As shown in Figure 6, oxidation kinetic follows a parabolic time dependence. At 500°C the oxidation rate is very low and the curves of the two materials are very similar. On the other hand, at 600°C, the oxidation rate is higher in case of WC-20Co. Parabolic constants, that were calculated as the higher slope of all curves, are reported in Table 4. The oxidation resistance of cemented carbide depends on the matrix amount and composition [17][18][19]. A decrease of the binder amount and a partial or complete substitution of Co with Ni lead to a reduced oxidation resistance. Oxidation kinetic highlights that the oxidation rate depends mainly on the matrix amount. As discussed above, a plausible interaction between TF and oxidation can be hypothesized. The cross sections and EDAX

analysis of the two materials after 3000 cycles highlight the inner oxidation of thermal cracks (Figure 7a and 7b).

Two types of oxide can be distinguished, namely a W-rich light grey oxide (WO_3), and a Co-rich dark grey oxide ($CoWO_4$). In case of WC-20Co the W-rich oxide mostly fills the deeper region of the crack while the Co-rich oxide covers the outermost crack surface. This behaviour is justified taking into account that the Co oxidation occurs before that of WC [16]. Differently, due to the presence of Ni, that is not able to moderate the rate of oxygen interaction with WC [14], a mixture of the two oxides is present into the crack of WC-30(CoNiCrFe). Increasing the binder amount, the WO_3 content decreases but, due to the presence of Ni, the amount of this oxide is higher than in the case of WC-30Co.

3.4 Correlation between TF and oxidation

WC-30Co seems to be characterized by a greater amount of oxide inclusions rather than cracks. This is due to the fact that the slower crack propagation induces a stronger interaction with oxidizing phenomena. Differently, cracks rich of oxide, but not oxide inclusions, are present on the surface of WC-20Co due to the higher crack propagation. Because of the higher oxidation kinetics, the WC-20Co oxidation at 600°C can be responsible, at least in part, for so high propagation rate. This statement is confirmed by the Pilling Bedworth ratio (PBR) [25] of WC-Co oxides, higher than unity [10][11][13][15], meaning that the volume expansion due to their formation inside the crack induces an additional tensile state at crack tip. The PBR of the two main WC-Co oxides, calculated using the equation (4), is equal to 3.33 in case of WO_3 and 2.25 in case of $CoWO_4$.

$$PBR_{M1_nM2_mO_x} = Vo/Vm = (MW_{M1_nM2_mO_x}/\lambda_{M1_nM2_mO_x}) \times (\delta_{M1}/n \times MW_{M1} + \delta_{M2}/m \times MW_{M2}) \quad (4)$$

where

$M1_nM2_mO_x$= generic oxide composed by two different metal M1 and M2

Vo and Vm = volume oxide and volume metal

MW = molecular weight

δ = density

The higher WO_3 PBR suggests, due to a greater volume expansion, an increased additional tensile state at crack tip when W-rich oxide is formed. For this reason it is possible to conclude that a higher propagation rate in the WC-20Co is firstly due to lower binder content but also due to higher oxidation rate and greater amount of W-rich oxide. From that, an oxide induced crack propagation mechanism is confirmed. Schematization of TF and oxidation behaviour of WC-20Co and WC-30(CoNiCrFe) is shown in Figure 7c.

4 Conclusions

The TF behaviour of cemented carbide was investigated. Two grades with different amount of binder, composition and WC grain size were studied. The overall conclusion of this study is that, firstly, the main propagation mechanism changes from an intergranular to a transgranular fracture of the WC increasing the WC grain size. Secondly, a decrease in the binder content leads to an increased propagation rate, avoiding the nucleation of new cracks due to a reduction in the local constraint close to the crack. Thirdly, an oxidation induced crack propagation mechanism is confirmed, especially in WC-20Co, due to a higher oxidation rate and W-rich oxide formation. From a practical point of view, is preferable to have a high crack density and low mean crack length. In fact, the removal of cracks by wear phenomena or grinding is easier in case of short cracks and the risk to have catastrophic failure is lower.

Figure captions

Figure 1: customary rig used for TF fatigue cracking (a). TF sample showing multiaxial stress state (T=tangential, A=axial) and multidirectional thermal cracking (b).

Figure 2: WC-20Co (a) and WC-30(CoNiCrFe) (b) SEM micrographs

Figure 3: surface thermal fatigue cracking for WC-20Co and WC-30(CoNiCrFe) after 1300 (a), 2000 (b) and 3000 (c) cycles

Figure 4: mean crack length (a) and crack density (b) vs number of cycles, correlation between mean crack length and crack density (c)

Figure 5: WC-20Co (a) and WC-30(CoNiCrFe) (b) penetration depth of thermal fatigue cracks after 3000 cycles, WC-20Co (c) and WC-30(CoNiCrFe) (d) propagation mechanisms after 3000 cycles

Figure 6: oxidation kinetics of WC-20Co and WC-30(CoNiCrFe) at 500 and 600°C

Figure 7: cross sections of WC-20Co (a) and WC-30(CoNiCrFe) (b) after 3000 cycles of thermal fatigue test and the oxide composition patterns, schematic representation of TF and oxidation behaviour changing the binder content (c)

Acknowledgments

The authors gratefully acknowledge Covi Danilo for the important contribution carried out in the experimental work.

References

[1] Santhanam AT, Tierney P, Hunt JL, Kennametal Inc. Cemented Carbides. In: ASM Int Handbook Committee. Properties and Selection: Non ferrous Alloys and Special Purpose Materials, ASM Handbook: The Materials Information Company; 1990, 2631-2688.

[2] Kenneth J.A. Brookes. Hardmetals and other Hard Materials. 2nd ed. Int Carbide Data 1992

[3] Gopal S. Upadhyaya. Mechanical Behaviour of Cemented Carbides. In: Cemented Tungsten Carbides: Production, Properties, and Testing, New Jersey: Noyes Publications; 1998, 193-226.

[4] Andrzej Weronski and Tadeusz Hejwowski. Thermal fatigue of metals: 1997

[5] Gopal S. Upadhyaya. Thermal Shock Resistance. In: Cemented Tungsten Carbides: Production, Properties, and Testing, New Jersey: Noyes Publications; 1998, 249-253.

[6] Tumanov VI, Gol’dberg ZA, Chernyshev VV, Pavlova ZI. Thermal shock resistance of tungsten carbide-cobalt alloys, Sov Powder Metall and Met Ceram 1966;5:818–822.

[7] Lagerquist M. A study of the thermal fatigue crack propagation in WC–Co cemented carbide. Powder Metall 1975;18:71–88.

[8] Ning L, Genying X, Yudong X. Thermal shock fatigue behaviours of cemented carbide YG20. Trans Nonferrous Met Soc China 1997;7:149-154.

[9] Ishihara S, Goshima T, Nomura K, Yoshimoto T. Crack propagation behaviour of cermets and cemented carbides under repeated thermal shocks by the improved quench test. J Mater Sci 1999;34:629– 636.

[10] Basu SN, Sarin VK. Oxidation behaviour of WC-Co. Mater Sci and Eng 1996; A209:206-212.

[11] Casas B, Ramis X, Anglada M, Salla JM, Lanes L. Oxidation-induced strength degradation of WC-Co hardmetals. Int J Refract Met Hard Mater 2001;19:303-309.

[12] Wang-Hoi Gu, Yeon Seok Jeong, Kyeongmi Kim, Jin-Chun Kim, Seong-Ho Son, Sunjung Kim. Thermal oxidation behaviour of WC-Co hard metal machining tool tip scraps. J Mater Process Technol 2012;212:1250-1256.

[13] Del Campo L, Pérez Sáez RB, González Fernández L, Tello MJ. Kinetics inversion in isothermal oxidation of uncoated WC-based carbides between 450 and 800°C. Corr Scie 2009;51:707-712.

[14] Voitovich VB, Sverdel VV, Voitovich RF, Golovko EI. Oxidation of WC-Co, WC-Ni and WC-Co-Ni Hard Metals in the Temperature Range 500-800°C. Int J Refract Met Hard Mater 1996;14:289-295.

[15] Bhaumik SK, Balasubramaniam R, Upadhyaya GS, Vaidya ML. Oxidation behaviour of hard and binder phase modified WC-10Co cemented carbides. J Mater Sci Lett 1992;11:1457-1459

[16] Liyong Chen, Danquing Yi, Bin Wang, Huiqun Liu, Chunping Wu, Xiang Huang, Huihui Li, Yuehong GaO. The selective oxidation behaviour of WC-Co cemented carbides during the early oxidation stage. Corr Sci 2015;94:1-5.

[17] Aristizabal M, Rodriguez N, Ibarreta F, Martinez R, Sanchez JM. Effect of the Binder Phase Content and Decarburization Phenomena on the Oxidation and Wear Resistance of WC-CoNiCr Materials. Manuscript refereed by Dr Henk Van Den Berg, Kennametal Technologies, Germany. Euro PM2009- Hard Mater III.

[18] Aristizabal M, Rodriguez N, Ibarreta F, Martinez R, Sanchez JM. phase sintering and oxidation resistance of WC-Ni-Co-Cr cemented carbides. Int J of Refractory Met Hard Mater 2010;28:516-522.

[19] Aristizabal M, Sanchez JM, Rodriguez N, Ibarreta F, Martinez R. Comparison of the oxidation behaviour of WC-Co and WC-Ni-Co-Cr cemented carbides. Corr Sci 2011;53:2754-2760.

[20] Gűnter Petzow. Metallographic Etching. ASM Int Mater Park 1999.

[21] E.G. Bennett and B. Roebuck. The Metallographic Measurement of WC Grain Size, NPL Good Pract Guide 1999;22:16-33.

[22] Engqvist H, Uhrenius B. Determination of the average grain size of cemented carbides. Int J Refract Met Hard Mater 2003;21:31-35.

[23] M. Pellizzari, D. Ugues and G. Cipolloni. Influence of heat treatment and surface engineering on thermal fatigue behaviour of tool steel. Int Heat Treat Surf Eng 2013;7:180-184.

[24] Minyoung Lee. High temperature hardness of tungsten carbide. Metallurgical Transactions A 1983;14:1625-1629 .[25] Pilling NB, Bedworth RE. The Oxidation of Metals at High Temperatures, J Inst Met 1923;29:529–582.

Highlights

- Transgranular/intergranular fracture of WC ratio changes, increasing the D_{WC}.
- The propagation rate decreases, increasing the binder content.
- The oxidation rate depends mainly on the matrix amount.
- An oxidation induced crack propagation mechanism is confirmed.

BINDER AMOUNT INFLUENCE ON THERMAL FATIGUE AND OXIDATION BEHAVIOURS IN CEMENTED CARBIDE

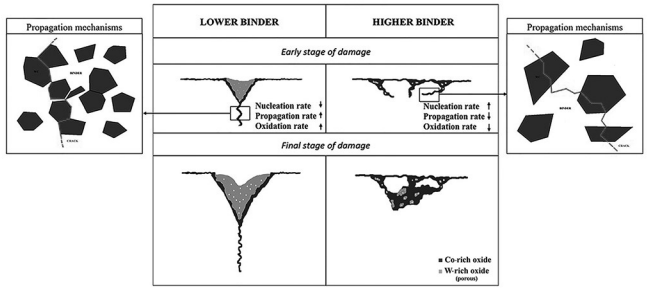

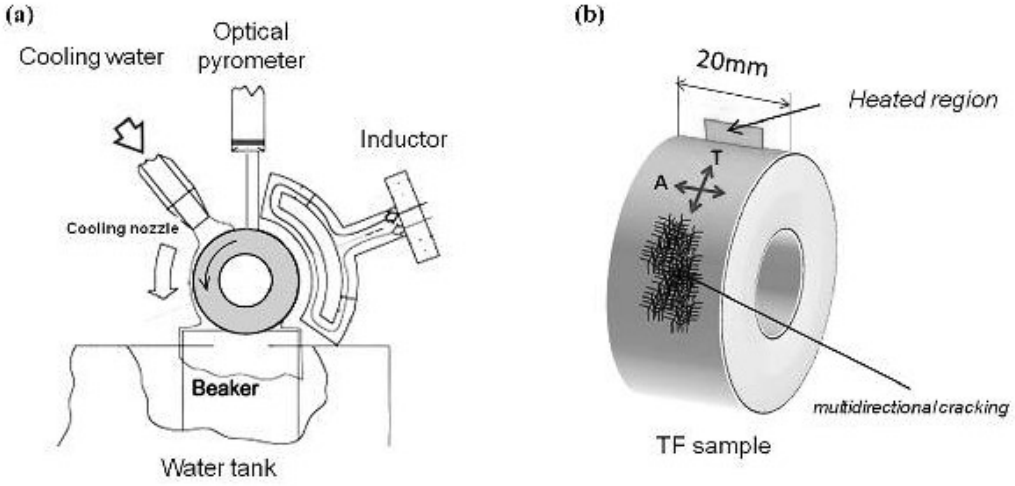
(a)
Cooling water
Optical pyrometer
Inductor
Cooling nozzle
Beaker
Water tank
(b)
20mm
Heated region
T
A
multidirectional cracking
TF sample

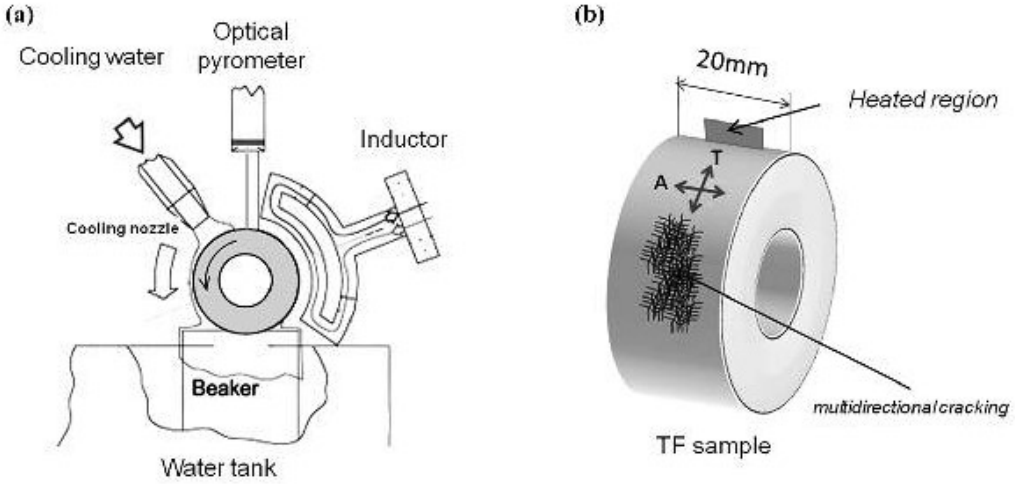
(a)
Cooling water
Optical pyrometer
Inductor
Cooling nozzle
Beaker
Water tank
(b)
20mm
Heated region
T
A
multidirectional cracking
TF sample

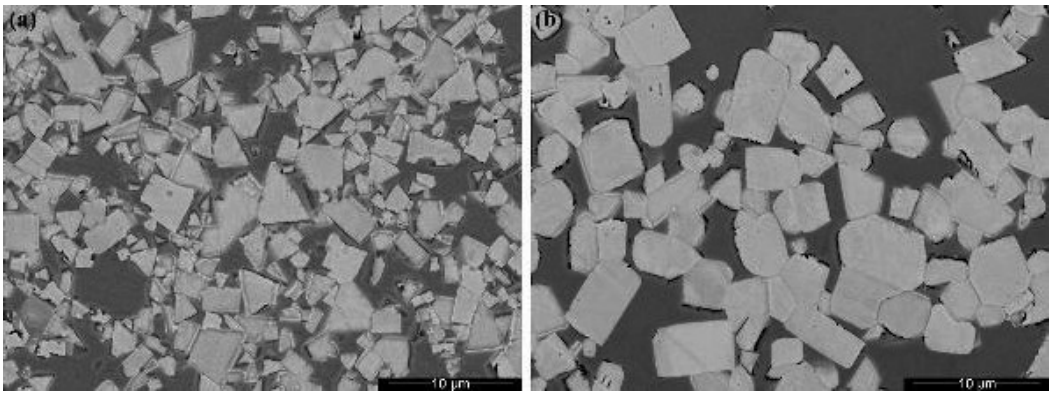
(a)
10 μm
(b)
10 μm

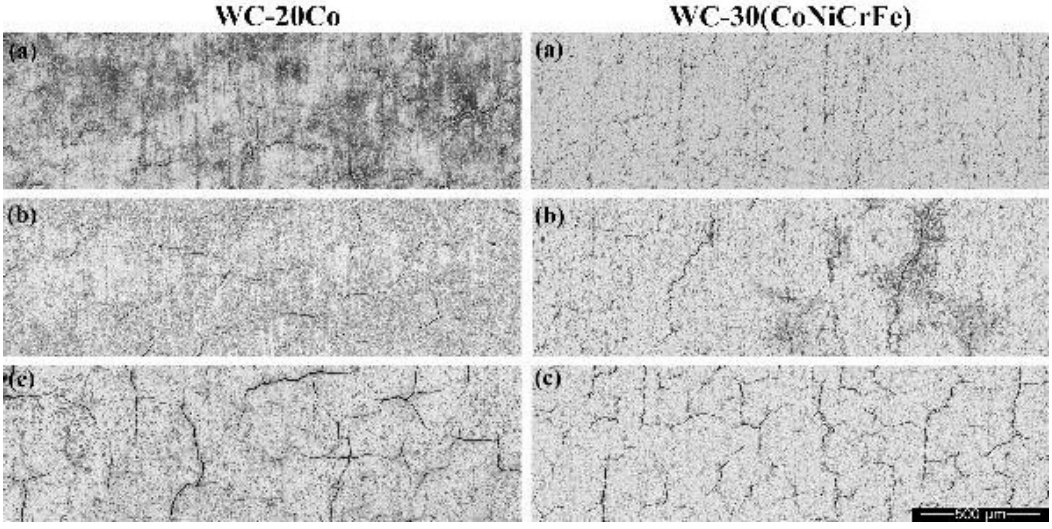
WC-20Co
WC-30(CoNiCrFe)
(a)
(b)
(c)
(a)
(b)
(c)
500 μm

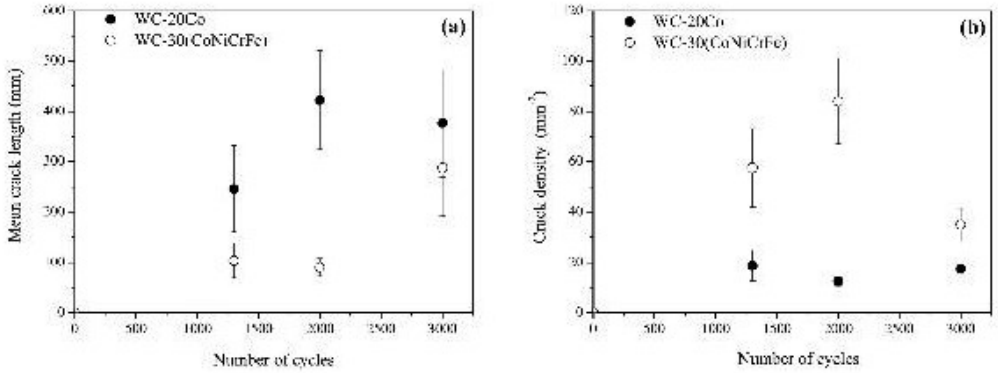
(a)
WC-20Co
WC-30(CoNiCrFe)
Mean crack length (mm)
Number of cycles
(b)
WC-20Co
WC-30(CoNiCrFe)
Crack density (mm⁻¹)
Number of cycles

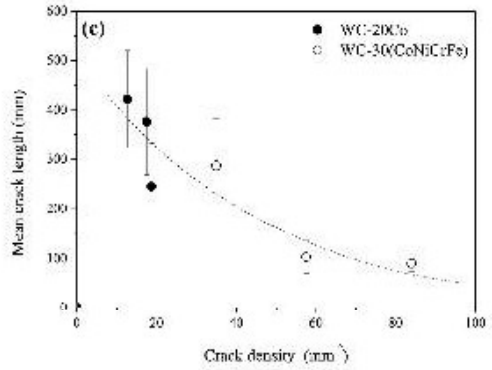
(c)
WC-20Co
WC-30(CoNiCrFe)
Mean crack length (mm)
Crack density (mm⁻¹)

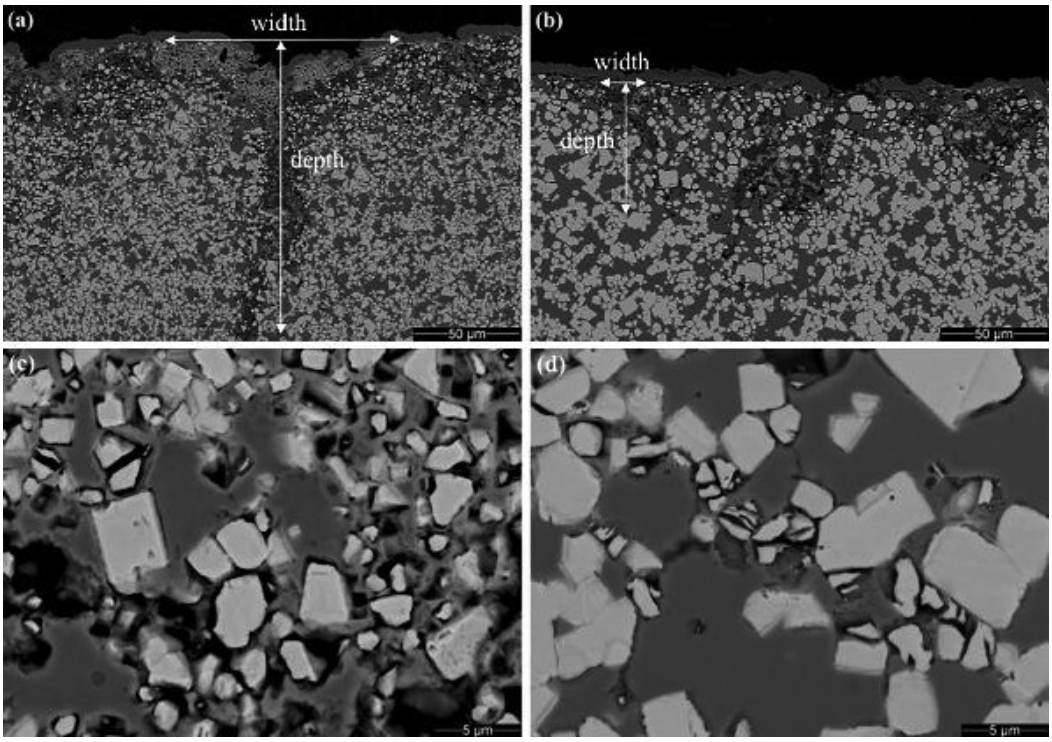
(a)
width
depth
50 µm
(b)
width
depth
50 µm
(c)
5 µm
(d)
5 µm

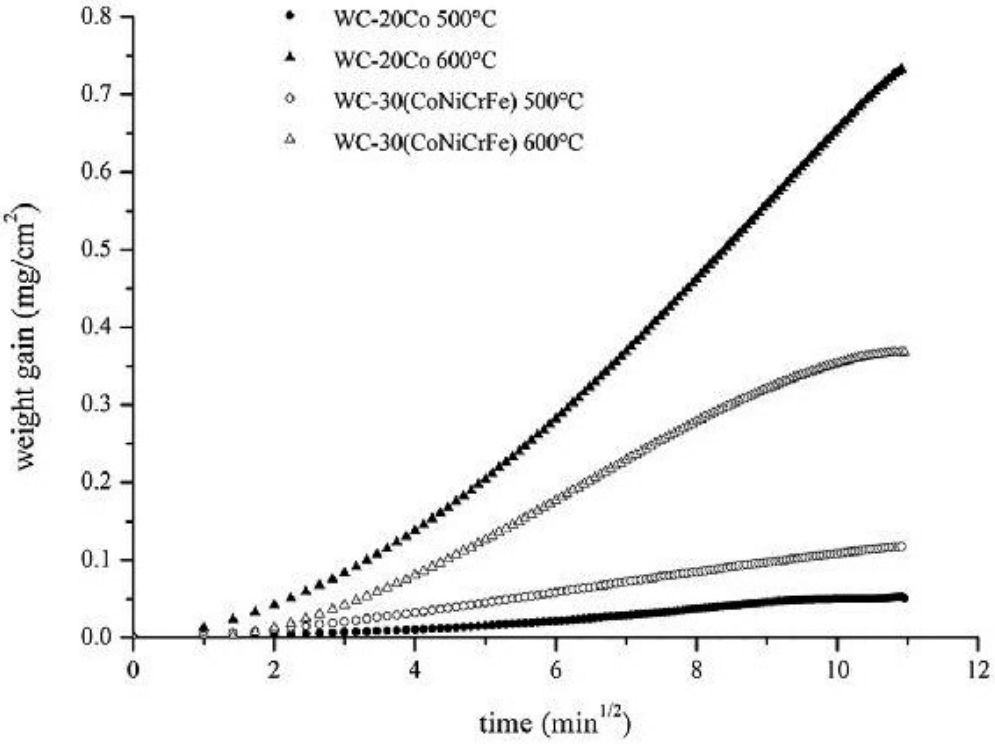
WC-20Co 500°C
WC-20Co 600°C
WC-30(CoNiCrFe) 500°C
WC-30(CoNiCrFe) 600°C
weight gain (mg/cm^2)
time (min$^{1/2}$)
0.0
0.1
0.2
0.3
0.4
0.5
0.6
0.7
0.8
0
2
4
6
8
10
12

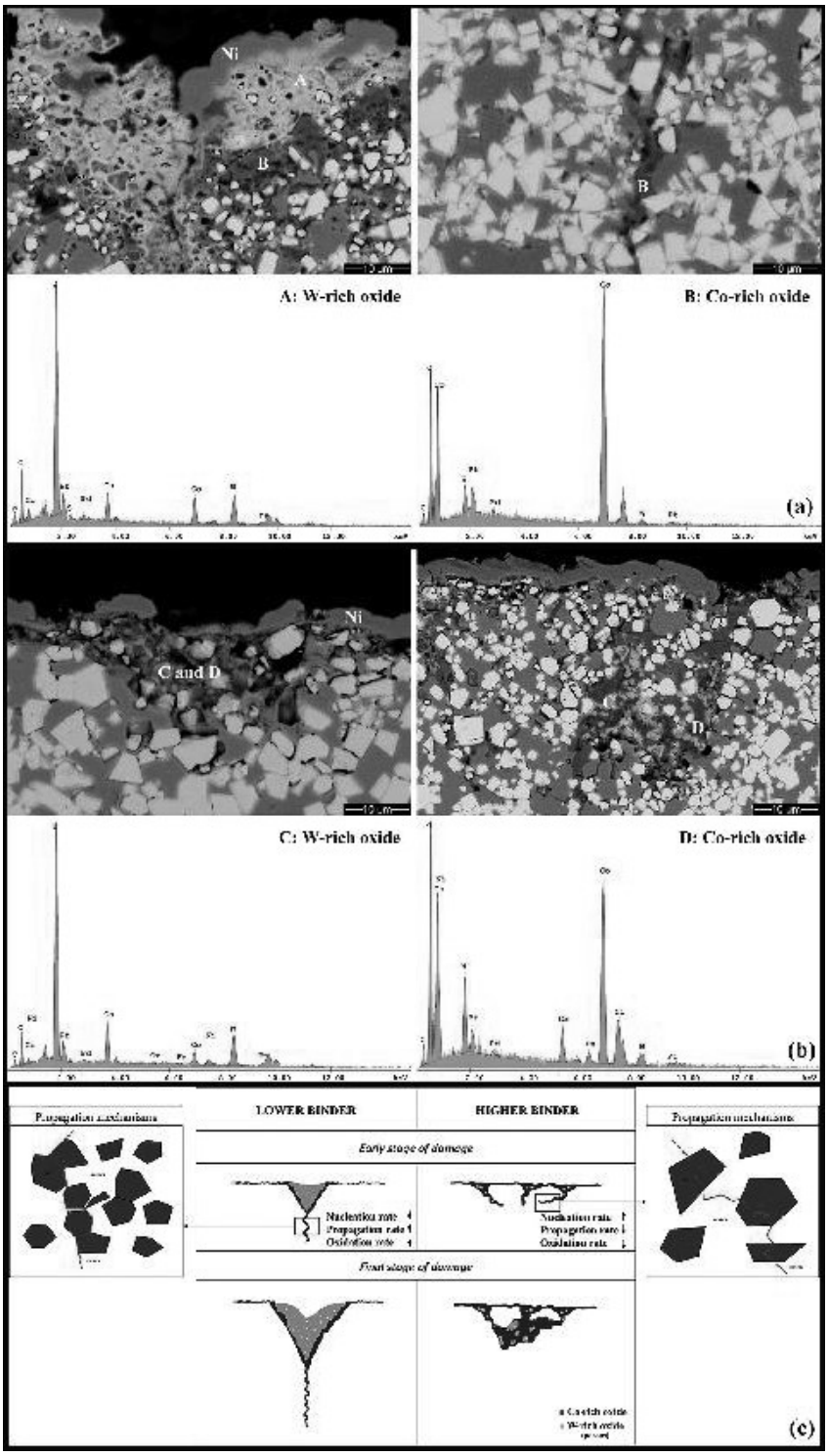
Ni
A
B
A: W-rich oxide
B: Co-rich oxide
(a)
Ni
C and D
C
D
C: W-rich oxide
D: Co-rich oxide
(b)
LOWER BINDER
HIGHER BINDER
Early stage of damage
Final stage of damage
(c)

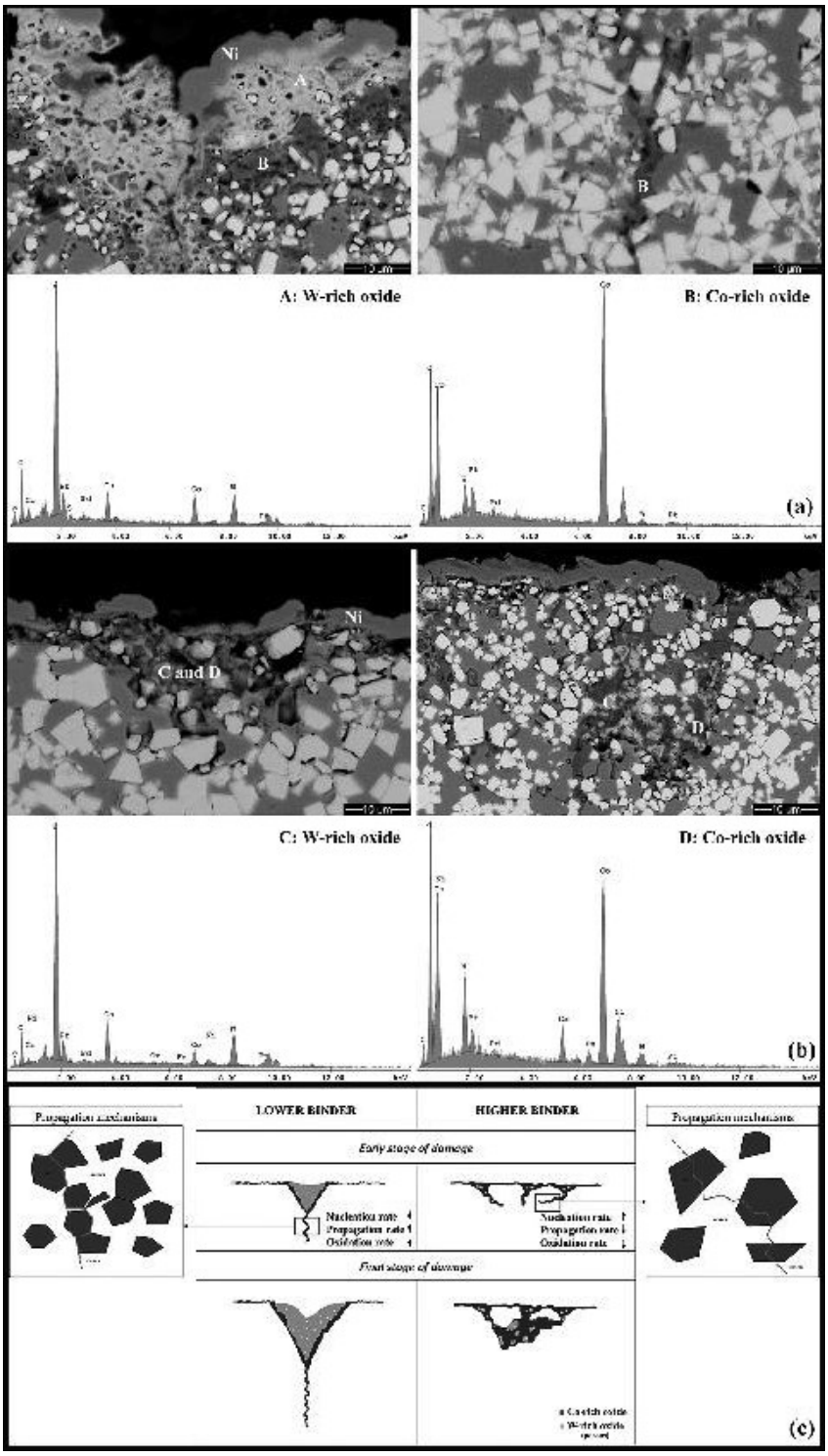
Ni
A
B
A: W-rich oxide
B: Co-rich oxide
(a)
Ni
C and D
C
D
C: W-rich oxide
D: Co-rich oxide
(b)
LOWER BINDER
HIGHER BINDER
Early stage of damage
Final stage of damage
(c)